ACS Macro Letters

Letter

pubs.acs.org/macroletters

Curvature-Driven Rigid Nanowire Orientation inside Nanotube Walls

Kiho Park, Kiwoon Choi, Joon Ho Lee, Sung Ho Park, Se Cheol Lee, and Han Sup Lee*

Department of Advanced Fiber Engineering, Inha University, 402-751, Incheon, Korea

Supporting Information

ABSTRACT: Self-aligning of a rigid hard domain nanowire inside the nanotube wall has been found for a segmented block copolymer, and applicability of the attenuated total reflection (ATR) technique of Fourier transform infrared (FTIR) spectroscopy to obtain quantitative three-dimensional orientation information of the nanowires in the nanotube has been demonstrated. The preferential orientation of a nanowire along a nanocylinder is explained in terms of the curvature of the nanotube and the persistence length of the hard domain nanowire. This observation may pave the way to new fabrication methods for the anisotropic performance of one-dimensional structures, such as electrical conductivity, piezoelectricity, and photonic properties of polymeric nanofibers and nanotubes.

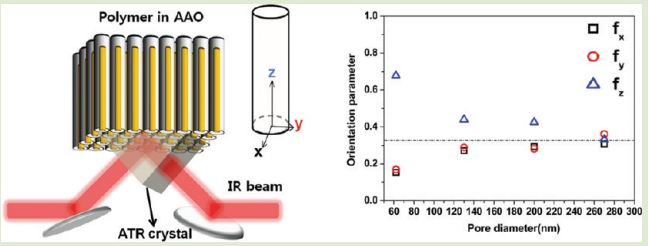

One-dimensional nanostructures, such as nanorods, nanofibers, and nanotubes of various polymeric materials, have attracted considerable attention in recent years due to the fundamental scientific interest and their potential applications to photonics, electronics, and mechanical and biomedical devices.[1−5] The physical properties of one-dimensional nanostructures are strongly affected by various morphology-forming processes, such as crystallization, chain orientation, and phase separation occurring under the effect of one-dimensional nanoconfinement.[6−14] Therefore, it can be a crucial step to understand/control the effect of nanoconfinement on the microstructure of the polymer materials to enhance/optimize the performance of the functional devices in a range of applications.

Many methods have been developed to fabricate well-defined, one-dimensional nanostructures, including template wetting, nanoimprint lithography, and microphase separation of block copolymer.[15−17] One-dimensional polymer nanostructures of high order and density can be prepared easily by infiltrating a polymer melt or solution into the pores of the nanoporous inorganic template, for example, anodized aluminum oxide (AAO).[15,16] Since the dimensions (length and diameter) of the straight cylindrical nanopores in AAO can be controlled precisely,[18] they have been used extensively to prepare one-dimensional polymer nanostructures and to examine the nano confinement effect on the microstructure of polymer materials.[6−11,14]

Compared to the polymer materials, many metal oxides, including aluminum oxide (AO), show relatively high surface tension. Therefore, the surface of AAO can be wetted easily with the polymer melt or solution.[15] The process of infiltration into one-dimensional nanopores in AAO with a polymer melt or solution are controlled by the pore size, process temperature, and spreading coefficient of polymer materials on the oxide surface.[6,16] Upon cooling, the polymer melt in nanopores in AAO, either nanorods or nanotubes of polymers, can be obtained depending on either partial or complete wetting phenomenon, respectively.[16] The drying of the polymer solution in nanopores is known to eventually leave the nanotube in AAO.[11] The spatial constraints imposed by the cylindrical nanopores on the one-dimensional polymer nanostructure would play a significant role in determining the microstructure forming process. Because the order and orientation of morphological units is strongly perturbed, the optical, mechanical, and electronic properties of the one-dimensional polymer material would be affected.

The effect of the curvature of a nanotube has been found to induce the anisotropic orientation of the two-dimensional lamellar crystal units. With poly(vinylidene fluoride) under nanotube confinement, it has been observed that the crystallites grow preferentially in the direction of minimum curvature on the surface of the nanotube.[11] In addition, studies on polyethylene confined within porous alumina membranes demonstrated that the anisotropic orientation of two-dimensional crystals has been developed, particularly when they were crystallized slowly. The *b*-axis of orthorhombic PE crystals was parallel to the long cylindrical axes of the nanopores, whereas *a*- and *c*-axes were almost in the plane perpendicular to the cylindrical axes.[7]

Although the nano confinement effect on the preferential orientation of the lamella crystals has been the subject of many studies, its effect on the preferential orientation of the one-dimensional domain has not been studied extensively. In this study, a polyurethane (PU) consisting of rigid one-dimensional hard domains dispersed in a soft matrix was infiltrated into the nanopores of AAO of various dimensions. The effect of the curvature of the nanotube on the anisotropic orientation of the rigid hard domain nanowires inside the nanotube wall was

Received: August 17, 2011
Accepted: November 2, 2011
Published: November 22, 2011

   dx.doi.org/10.1021/mz200026g | *ACS Macro Lett.* 2012, 1, 110−114

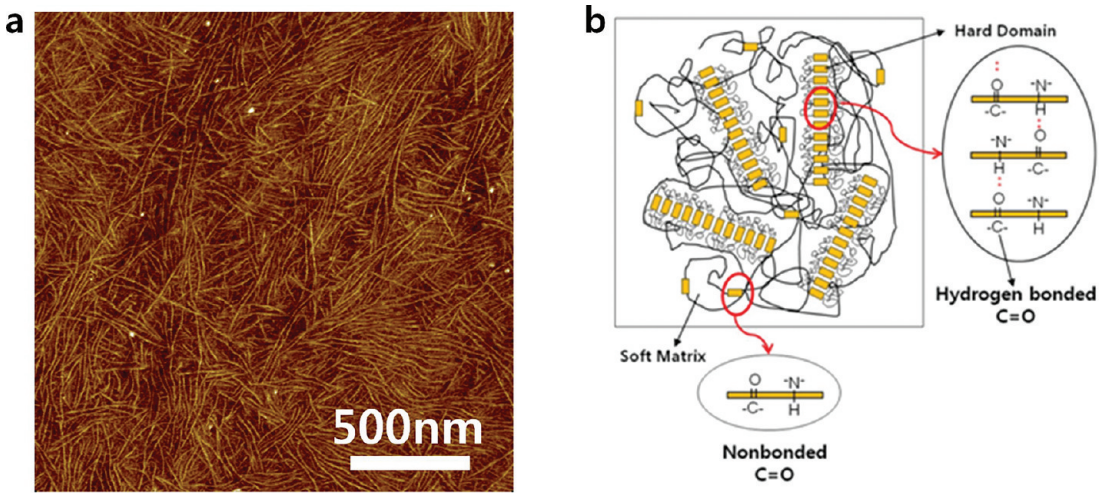

Figure 1. PPDI-based PU film. (a) AFM tapping image. The bright nanowires correspond to the hard domains and the dark surrounding is the soft matrix. (b) Schematic of the phase separated PPDI-based PU. The hard domain consists of hard segments bonded strongly to each other through hydrogen bonding between the C═O and N−H groups. The hard segments dispersed in the soft matrix show a nonbonded C═O group.

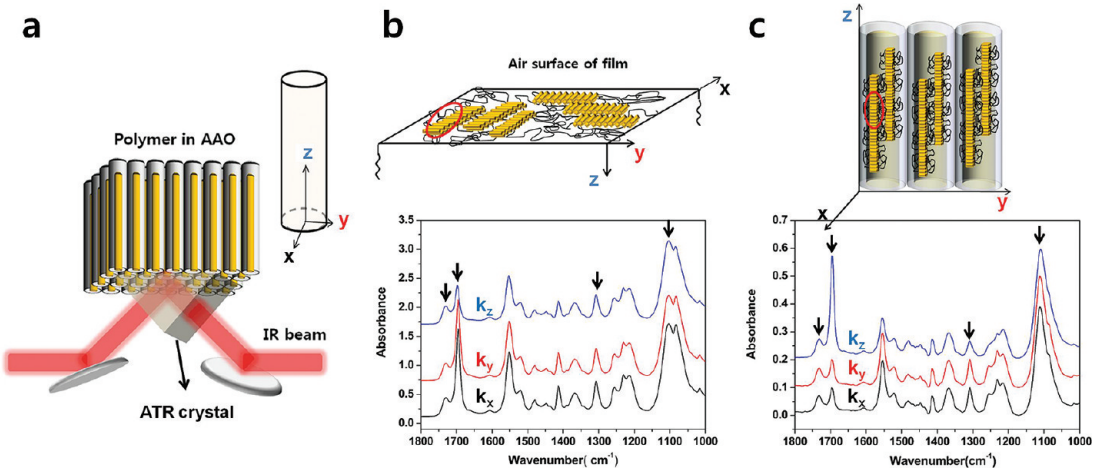

Figure 2. ATR setup and attenuation index spectra. (a) Schematic diagram showing the relative orientation of the nanotube sample and ATR crystal. Three attenuation index spectra of the PPDI-based film (b) and nanotube samples (c). Schematic diagram showing the nanowire orientation in the two samples (film, nanotube) at the top of the attenuation index spectra.

studied by FTIR spectroscopy using the ATR method and atomic force microscopy (AFM).

The polyurethane used in this study was a segmented block copolymer consisting of hard and soft segments with very different physical properties. Owing to the thermodynamic incompatibility between the two segments, they undergo a microphase separation process resulting in the heterogeneous domain structure. Rigid hard domain nanowires with a high aspect ratio were dispersed in the soft domain matrix.[19] (Figure 1a) Based on the AFM image and small-angle X-ray scattering (SAXS) data (not shown), the thickness of the hard domain nanowires was estimated to be approximately 10 nm. As shown schematically in Figure 1b, the hard segments inside the hard domain are perpendicular to the long axis of the hard domain nanowires. Therefore, the hydrogen bonding direction between the carbonyl group and N−H group is parallel to the longitudinal direction of the nanowire. Because the relative distribution of hydrogen bonding along three orthogonal directions (x, y, z) can be examined by FTIR-ATR,[20−24] information on the preferential orientation of the hard domain nanowire inside the wall of the nanotubes of various dimensions could be obtained.

Figure 2a shows the schematic showing the relative orientation of the nanotube sample at the interface with the ATR crystal. The preparation process of the nanotube polymer sample is explained in the Supporting Information (Preparation of PU nanotube for FTIR-ATR measurement). With this setup and careful analysis process explained in the Supporting Information (3D orientation analysis using FTIR-ATR), the three-dimensional orientation information of the hard domain nanowire along the three orthogonal directions could be obtained.

Figure 2b and c show the attenuated index spectra (k_x, k_y, k_z) obtained along three orthogonal directions of the thin film (Figure 2b) and of the nanotubes in AAO with 60 nm diameters (Figure 2c). In the case of a thin film (Figure 2b), the k_z component (out-of-plane component) of the 1700 cm^{-1} peak attributed to the hydrogen-bonded carbonyl stretching vibration[25] was relatively small compared to the corresponding k_x, k_y components (in-plane components). On the other hand, in the case of the nanotube (Figure 2c), the k_z component

dx.doi.org/10.1021/mz200026g | ACS Macro Lett. 2012, 1, 110−114

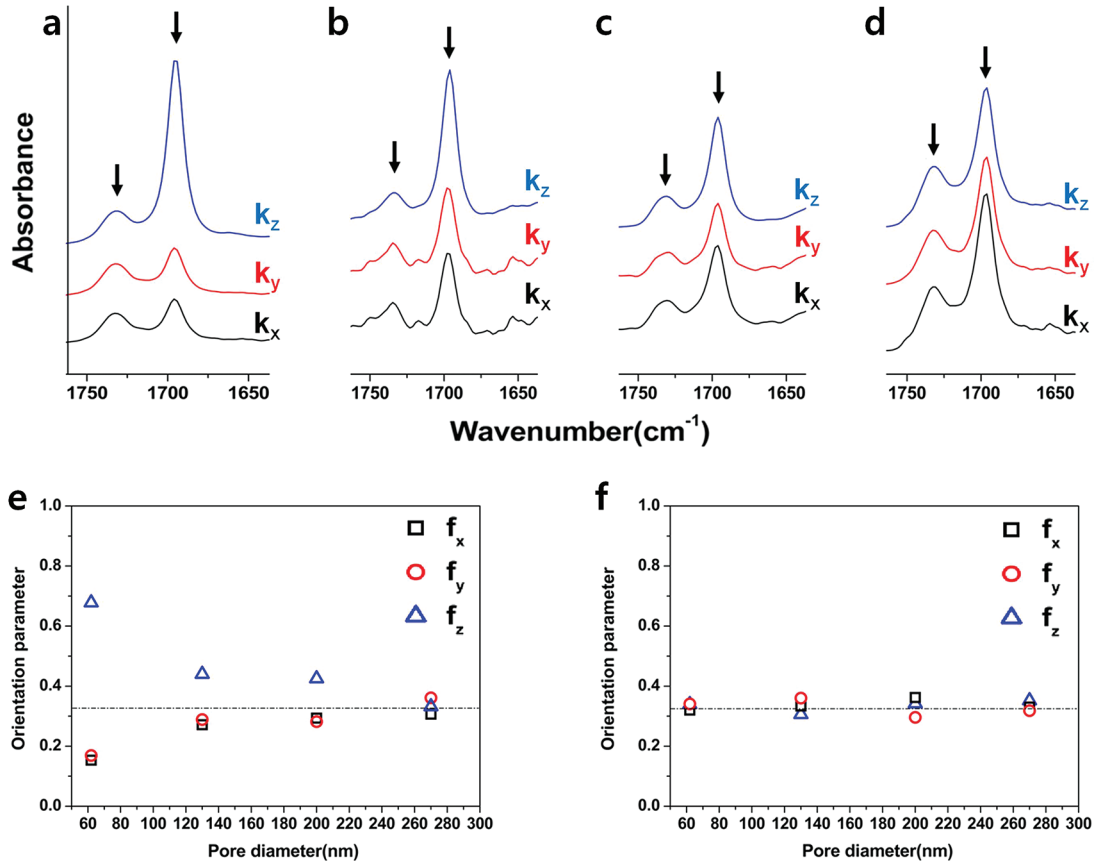

Figure 3. Attenuation index spectra and orientation parameter. Carbonyl stretching region of the attenuation index spectra obtained using nanotube samples with (a) 60, (b) 130, (c) 200, and (d) 270 nm diameters. Orientation parameters along three orthogonal directions of (e) hydrogen-bonded and (f) nonbonded C═O stretching peaks.

(longitudinal direction of the cylindrical pore) is significantly greater than the k_y, k_z component (radial directions of the cylindrical pore). This intensity difference between three orthogonal components is indicative of the preferential orientation of the hard domain nanowires, as shown schematically at the top of Figure 2b and c for the thin film and nanotube, respectively. For the hard domain nanowires in the AAO nanotube, the hydrogen bonded carbonyl stretching peak at 1700 cm^{-1} was along the longitudinal direction of the nanotube, which was measured with the k_z component in Figure 2c.

To examine the effect of the curvature of the nanotubes in AAO on the preferential orientation of the hard domain nanowires, three attenuation index spectra were obtained with nanotubes in AAO with various diameters ranging from 60 to 270 nm, and the carbonyl group stretching regions are shown in Figure 3a–d. The relative intensity of the carbonyl peak at 1700 cm^{-1} to that at 1730 cm^{-1} changes continuously with the increasing diameter of the nanotube in AAO.

The preferential orientation of the hard domain nanowire can be expressed quantitatively with the orientation parameters along three orthogonal directions (refer to 3D orientation analysis using FTIRT-ATR in Supporting Information). The orientation parameters of the hard domain nanowire were obtained from the hydrogen bonded carbonyl peak at 1700 cm^{-1} and the ones of the soft matrix surrounding the nanowires were obtained from the nonbonded carbonyl peak at 1730 cm^{-1}, and the results are shown in Figure 3e and Figure 3f, respectively. For the hard domain nanowire, 60 nm in diameter, the orientation parameter along the z direction (f_z) is significantly greater than the corresponding two radial components (f_x, f_y). On the other hand, the difference between these components becomes gradually smaller with increasing diameter of the nanotube in AAO. The difference became almost negligible as the nanotube diameter reached approximately 270 nm. This suggests that the preferential orientation of the rigid hard domain nanowires along the axial direction of the nanotube observed with the sample, 60 nm in diameter, becomes progressively smaller with increasing nanotube diameter. The hard domain nanowires were almost randomly oriented inside the 270 nm diameter nanotube.

The orientation of the soft matrix surrounding the hard domain nanowire can be estimated from the orientation parameters (f_x, f_y, f_z) of the nonbonded carbonyl stretching peak at 1730 cm^{-1}, which are shown in Figure 3f. The almost identical orientation parameters irrespective of the three orthogonal directions for all nanotubes examined indicate that no significant anisotropy can be observed in the case of the soft matrix surrounding the hard domain nanowires. The preferential orientation of the hard domain nanowires along the axial direction of nanotubes in AAO, particularly the relatively smaller diameter sample, appears to be related to the rigidity of the hard domain nanowires.

Figure 4a shows a schematic diagram of the cross-sectional shape of the nanotube in AAO. Because the concentration of the polymer solution infiltrated into the AAO was approximately 20% (w/w), the inner radius (r_i) of the nanotube can be related to the outer radius (r_o) as $((r_i)/(r_o)^2) \cong 0.8$. The

dx.doi.org/10.1021/mz200026g | *ACS Macro Lett.* 2012, 1, 110–114

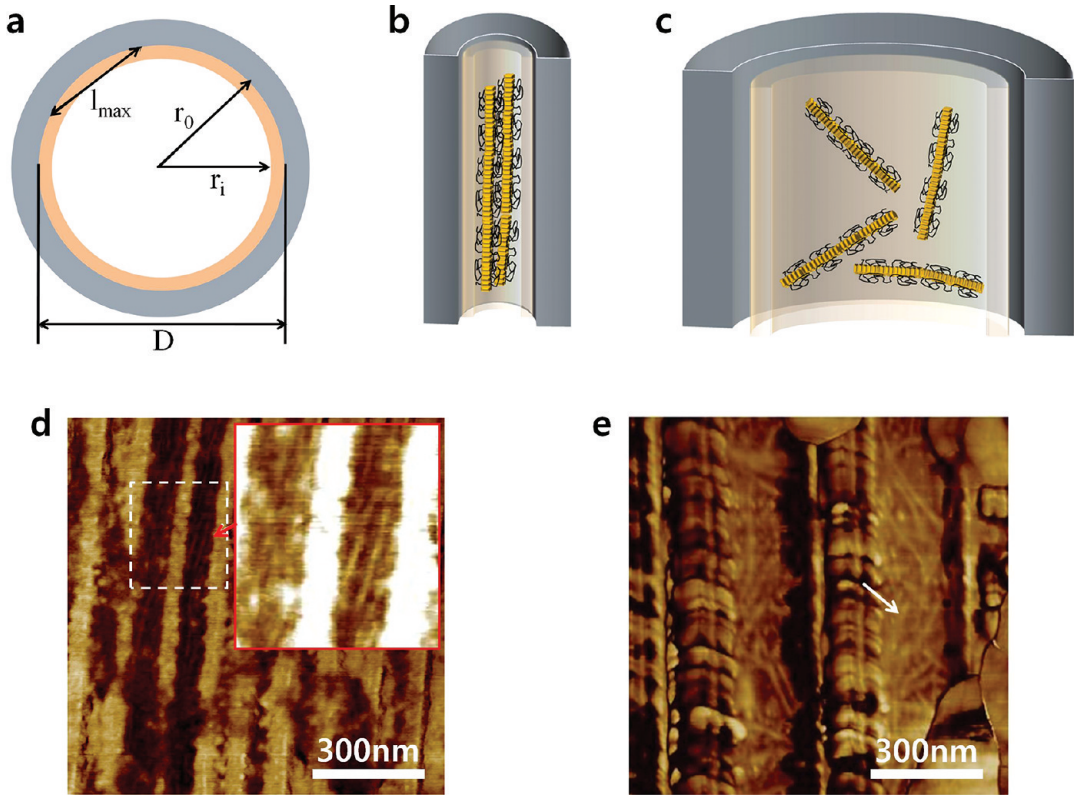

Figure 4. Nanowire orientation in the nanotube with small and large diameters. (a) Cross sectional shape of the nanotube. Schematics showing the nanowire alignment in nanotube of (b) 60 and (c) 270 nm diameter. (d) AFM phase image of 60 nm diameter sample. Portion of the image is reprocessed to enhance the contrast of oriented nanowires and added in the inset. Bright area corresponds to AAO. (e) AFM phase image of 270 nm diameter sample. White arrow in (e) indicates the hard domain nanowire.

maximum chord length (l_{max}) that can reside along the radial direction of the nanotube was approximately $0.89r_o$. For the nanotubes used in this study, l_{max} ranged from 54 to 243 nm.

If the persistence length (l_{per}) of the hard domain nanowire was greater than l_{max}, the growth of the hard domain nanowire along the radial direction during the phase separation process would be retarded significantly compared to the one along the longitudinal direction. The preferential orientation of the hard domain nanowire along the longitudinal direction, as shown schematically in Figure 4b, appears to indicate that the persistence length of the nanowire is longer than the l_{max} of the 60 nm diameter nanotube. If $l_{max} > l_{per}$, the hard domain nanowires may be oriented randomly inside the nanotube wall, as shown schematically for the 270 nm diameter nanotube in Figure 4c.

Although the persistence length of the flexible polymer chain is approximately several nanometers, it was reported to reach as high as 50 nm for rigid double helix DNA molecules.[26,27] As shown in Figure 1b, the hard domain nanowires consist of hard segments strongly hydrogen bonded along the long axis of the nanowire. Figure 3e indicates that l_{per} of hard domain nanowire is longer than 54 nm but shorter than 243 nm.

The hard domain nanowires can be observed from AFM images for two nanotubes, 60 and 270 nm in diameter, and the results are shown in Figure 4d and f. The thin layer of the AAO containing polymer nanotubes was sliced with a razor blade and the inner surface of the nanotubes was apparently monitored by AFM. In the case of the nanotube in the AAO, 60 nm in diameter, the preferential orientation of nanowires along the longitudinal direction of the nanotube wall was clearly confirmed, as expected (Figure 4d). In addition, the random orientation of the hard domain nanowire for the nanotube, 270 nm in diameter, can also be observed (Figure 4e). AFM observation supports that the curvature of the nanotube might be a major factor determining the preferential orientation of the rigid nanowires inside the nanotube walls.

In summary, this study examined the effect of the nanotube curvature on the preferential orientation of the hard domain nanowire. The preferential orientation of the rigid nanowire and the flexible matrix surrounding the nanowire was evaluated quantitatively by applying the total reflection of the infrared radiation at the interface between the ATR crystal (diamond) and nanotube ends. The longitudinal orientation of the nanowire inside the nanotube with a smaller diameter and the random orientation inside the nanotube with a larger diameter were confirmed by AFM, and the results are interpreted in terms of the relative magnitude of the persistence length of the hard domain nanowire compared to the maximum radial chord length inside the nanotube. This study establishes a major parameter self-aligning the rigid nanowire inside one-dimensional nanostructure that can be used to secure the anisotropic electrical, photonic, and electromechanical properties of the nanofiber and nanotube.

■ EXPERIMENTAL METHODS

Fabrication of PU nanotube in AAO: A 20 wt % PU solution was dropped on the top on the AAO disk (preparation method of AAO is explained in the Supporting Information). The PU solution was infiltrated into the pores of AAO by wetting the pore surface. After drying for 24 h, the AAO with PU in the pores was heated to 200 °C under vacuum to remove any anisotropy that might be developed

dx.doi.org/10.1021/mz200026g | *ACS Macro Lett.* 2012, 1, 110−114

during the shear flow of the PU solution into the pores. The AAO was then heat treated at 80 °C again for 24 h to establish the phase-separated morphology.

AFM analysis: Atomic force microscopy (AFM) was performed with a Dimension NanoScope III. An aluminum substrate of AAO containing PPDI-based polyurethane sample in the pore was dissolved with $CuCl_2 \cdot 2H_2O$ + HCl solution. The remaining alumina disk was cut with a razor blade and the sliced surface was monitored by AFM, operating in tapping mode, to obtain Figure 4d,e.

FTIR-ATR spectroscopy: The FTIR spectra were obtained using VERTEX 80v vacuum FTIR spectrometer (Bruker) equipped with single reflection diamond ATR setup (Pike) and DTGS detector. Infrared radiation polarized either along the TE (transverse electric) direction or along TM (transverse magnetic) direction was used by inserting the automatic rotatable wire grid polarizer between the ATR setup and detector. Thirty two scans were averaged to obtain FTIR spectra with a 4 cm^{-1} resolution.

■ ASSOCIATED CONTENT

Supporting Information

A detailed description of the experimental methods and additional experimental results. This material is available free of charge via the Internet at http://pubs.acs.org.

■ AUTHOR INFORMATION

Corresponding Author

*Tel.: 82-32-860-7495. Fax: 82-32-873-0181. E-mail: hslee@inha.ac.kr.

Notes

The authors declare no competing financial interest.

■ ACKNOWLEDGMENTS

This study is supported by Basic Science Research Program through the National Research Foundation of Korea (NRF) funded by the Ministry of Education, Science and Technology (Grant 2010-0024153)

■ REFERENCES

(1) Kabashin, A. V.; Evans, P.; Pastkovsky, S.; Hendren, W.; Wurtz, G. A.; Atkinson, R.; Pollard, R.; Podolskiy, V. A.; Zayats, A. V. *Nat. Mater.* **2009**, *8*, 867−871.
(2) HU, Z.; Tian, M.; Nysten, B.; Jonas, A. M. *Nat. Mater.* **2009**, *8*, 62−67.
(3) Haberkorn, N.; Gutmann, J. S.; Patrick, T *ACS Nano* **2009**, *3*, 1415−1422.
(4) Caroll, O. D.; Lieberwirth, I.; Redmond, G. *Nat. Nanotechnol.* **2007**, *2*, 180−184.
(5) Choi, K.; Park, S. H.; Song, Y. M.; Lee, Y. T.; Hwangbo, C. K.; Yang, H.; Lee, H. S. *Adv. Mater.* **2010**, *22*, 3713−3718.
(6) Steinhart, M.; Göring, P.; Dernaika, H.; Prabhukaran, M.; Gösele, U.; Hempel, E.; Thurn-Albrecht, T. *Phys. Rev. Lett.* **2006**, *97*, 027801.
(7) Shin, K.; Woo, E.; Jeong, Y. G.; Kim, C.; Huh, J.; Kim, K. W. *Macromolecules* **2007**, *40*, 6617−6623.
(8) Duran, H.; Steinhart, M.; Butt, H. J.; Flouadas, G. *Nano Lett.* **2011**, *11*, 1671−1675.
(9) Xiang, H.; Shin, K.; Kim, T.; Moon, S. I.; McCarthy, T. J.; Russell, T. P. *Macromolecules* **2004**, *37*, 5660−5664.
(10) Wu, H.; Wang, W.; Yang, H.; Su, Z. *Macromolecules* **2007**, *40*, 4244−4249.
(11) Steinhart, M.; Senz, S.; Wehrspohn, R. B.; Gösele, U.; Wendorff, j. H. *Macromolecules* **2003**, *36*, 3646−3651.
(12) Ok, S.; Steinhart, M.; Serbescu, A.; Franz, C.; Vaca Chávez, F.; Saalwächter, K. *Macromolecules* **2010**, *43*, 4429−4434.
(13) Stewart-Sloan, C. R.; Thomas, E. L. *Eur. Polym. J.* **2011**, *47*, 630−646.
(14) Wang, Y.; Qin, Y.; Berger, A.; Yau, E.; He, C. C.; Zhang, L. B.; Gosele, U.; Knez, M.; Steinhart, M. *Adv. Mater.* **2009**, *21*, 2763−2766.
(15) Steinhart, M.; Wendorff, J. H.; Greiner, A.; Wehrspohn, R. B.; Nielsch, K.; Schilling, J.; Choi, J.; Göesele, U. *Science* **2002**, *296*, 1997.
(16) Zhang, M.; Dobriyal, P.; Chen, J. T.; Russell, T. P. *Nano Lett.* **2006**, *6*, 1075−1079.
(17) Lee, J. I.; Cho, S. H.; Park, S.-M.; Kim, J. K.; Kim, J. K.; Yu, J.-W.; Kim, Y. C.; Russell, T. P. *Nano Lett.* **2008**, *8*, 2315−2320.
(18) Masuda, H.; Fukuda, K. *Science* **1995**, *268*, 1466−1468.
(19) Sheth, J. P.; Klinedinst, D. B.; Wilkes, G. L.; Yilgor, I.; Yilgor, E. *Polymer* **2005**, *46*, 7317−7322.
(20) Flournoy, P. A.; Schaffers, W. J. *Spectrochim. Acta* **1966**, *22*, 5−13.
(21) Flournoy, P. A. *Spectrochim. Acta* **1966**, *22*, 15−20.
(22) Mirabella, F. M. *Appl. Spectrosc.* **1988**, *42*, 1258−1265.
(23) Walls, D. J. *Appl. Spectrosc.* **1991**, *45*, 1193−1198.
(24) Liang, Y.; Lee, H. S. *Macromolecules* **2005**, *38*, 9885−9888.
(25) Yilgor, I.; Yilgor, E.; Guler, I. G.; Ward, T. C.; Wilkes, G. L. *Polymer* **2006**, *47*, 4105−4114.
(26) Tinland, B.; Pluen, A.; Sturm, J.; Weill, G. *Macromolecules* **1997**, *30*, 5763−5765.
(27) Geggier, S.; Kotlyar, A.; Vologodskii, A. *Nucleic Acids Res.* **2010**, *39*, 1419−1426.